Understanding the Photochemical Properties of Polythiophene Polyelectrolyte Soft Aggregates with Sodium Dodecyl Sulfate for Antimicrobial Activity

Livshits, Maksim Yuryevich
Yang, Jianzhong
Maghsodi, Fahimeh
Strach, Edaward
Brown, Dylan
Scheberl, Andrea
Reimhult, Erik
Rack, Jeffrey J.
Whitten, David G.

Understanding the Photochemical Properties of Polythiophene Polyelectrolyte Soft Aggregates with Sodium Dodecyl Sulfate for Antimicrobial Activity

Maksim Y. Livshits,* Jianzhong Yang, Fahimeh Maghsoodi, Andrea Scheberl, Samuel M. Greer, Mohammed I. Khalil, Edward Strach, Dylan Brown, Benjamin W. Stein,* Erik Reimhult,* Jeffrey J. Rack,* Eva Chi,* and David G. Whitten*

Cite This: https://doi.org/10.1021/acsami.1c18553

Read Online

ACCESS | Metrics & More | Article Recommendations | Supporting Information

ABSTRACT: The threat of antibiotic-resistant bacteria is an ever-increasing problem in public health. In this report, we examine the photochemical properties with a proof-of-principle biocidal assay for a novel series of regio-regular imidazolium derivative poly-(3-hexylthiophene)/sodium dodecyl sulfate (P3HT-Im/SDS) materials from ultrafast sub-ps dynamics to μs generation of reactive oxygen species (ROS) and 30 min biocidal reactivity with *Escherichia coli* (E. coli). This broad series encompassing pure P3HT-Im to cationic, neutral, and anionic P3HT-Im/SDS materials are all interrogated by a variety of techniques to characterize the physical material structure, electronic structure, and antimicrobial activity. Our results show that SDS complexation with P3HT-Im results in aggregate materials with reduced ROS generation and light-induced anti-microbial activity. However, our characterization reveals that the presence of non-aggregated or lightly SDS-covered polymer segments is still capable of ROS generation. Full encapsulation of the P3HT-Im polymer completely deactivates the light killing pathway. High SDS concentrations, near and above critical micelle concentration, further deactivate all anti-microbial activity (light and dark) even though the P3HT-Im regains its electronic properties to generate ROS.

KEYWORDS: reactive oxygen species (ROS), poly-(3-hexylthiophene) (P3HT), imidazolium, sodium dodecyl sulfate (SDS), *Escherichia coli* (E. coli), ultraviolet visible irradiation and polymer aggregate material
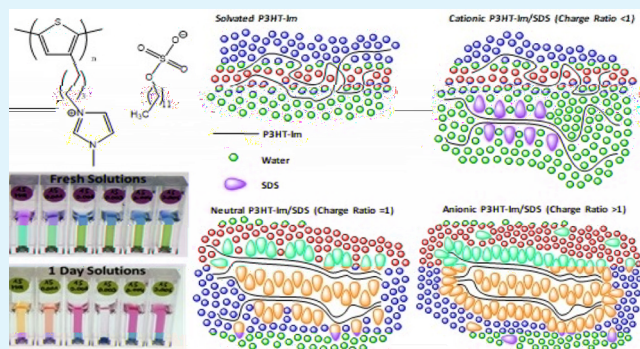
INTRODUCTION

Bacterial resistance to traditional small-molecule antibiotic treatments is an ever-increasing problem in today's world.[1–3] The rapid increase is attributable to the slow development of novel antimicrobial agents and the rapid evolution of bacteria. Bacteria are known to have many defense systems against antibiotics that enable the bacteria to modify drug protein targets,[4,5] generate neutralization agents for known antibiotics,[6,7] or adapt protein efflux pumps[8–10] to quickly remove the antibiotic from within the cell envelope. This has led scientists to look for new alternative anti-bacterial strategies. A broad range of therapies (**ex situ** contact killing,[11–13] photodynamic therapy (PDT),[14–16] and targeted radio-therapies)[17,18] are being explored as alternative anti-bacterial strategies for their ability to trigger bacterial death through non-specific cell killing pathways.

In the PDT, water-soluble, metal-free conjugated polyelectrolytes are an emerging field of interest. For example, water-soluble porphyrin oligomers,[19,20] push–pull donor–acceptor conjugated polymers,[21–23] and polythiophene-conjugated

polymer derivatives[24,25] exhibit many attractive properties for PDT and anti-bacterial therapies due to their large absorbance cross-sections, fluorescence, and sensitizing abilities, especially in the production of reactive oxygen species (ROS) including peroxides, singlet oxygen, and hydroxyl radicals. Most importantly, "push–pull" donor–acceptor and polythiophene-conjugated polymers are solution processable, easily tunable material platforms for bacterial targets by modification of side functional groups or incorporation into block co-polymers.[23]

Synthetic functional group modifications pendant to the backbone of conjugated polyelectrolytes (specifically polythiophenes) can be used to tune the electronic properties and

the aggregation behavior of the bulk material.[26−28] Understanding the aggregation properties of polythiophene materials has been an important ongoing challenge for tailoring material performance in a given application. For instance, controlling π-stacking in regio-regular poly(3-hexylthiophene-2,5-diyl) aggregates from long linear chains (J-type aggregates) to other non-linear geometries (H-type aggregates) has been demonstrated to change the nature of excited state deactivation and triplet excited state formation important in organic light harvesting systems and the broader class of organic optical electronics.[28−30] Likewise, hyperpolarizability of polythiophene aggregates with long alkyl chains [>12 repeat units (n)] in the presence of a magnetic field has also been shown to exhibit Faraday rotations and large Verdet constants in organic magneto-optical materials.[31] Donor−acceptor functionalization of thiophene polymers using cyanoacrylate functional groups has been demonstrated to decrease the crystallinity of the thiophene material, while turning on a local charge transfer interaction orthogonal to the polymer backbone.[32]

Recently, the synthesis, photophysical properties, and biocidal activity of a regio-regular head-to-tail polythiophene substituted with cationic imidazolium units (P3HT-Im) prepared by Grignard metathesis controlled polymerization was reported (Scheme 1).[33] In water, P3HT-Im has a broad

Scheme 1. Bond Line Structures of P3HT-Im and SDS (Left)[a]
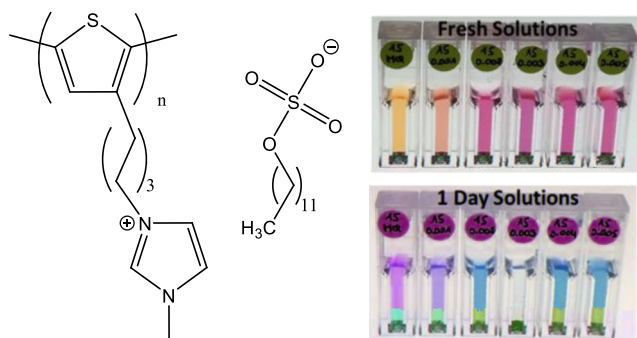
[a]Imaged series of 10 μg/mL P3HT-Im/SDS solutions taken shortly and 1 day after preparation (right, charge mole ratios are shown in Table 1).

absorption in the visible region and exhibits a remarkably high biocidal efficiency with both Gram-positive and Gram-negative bacteria at low 1−10 μg/mL concentrations.[33] Studies with mammalian cells suggest that P3HT-Im is nontoxic to these cells at concentrations ≤20 μg/mL over a short time scale (≤1 h) in the dark and light.[34] This study demonstrates the capability of P3HT-Im to achieve selective imaging and inactivation of bacteria over mammalian cells, suggesting that the polymer has significant potential for defeating antibiotic-resistant bacteria. More recently, we have found that a series of P3HT oligomers and polymers are effective against a panel of Gram-positive and Gram-negative bacteria including two Eskape pathogens.[35] Our investigations of the biocidal activity of the cationic P3HT-Im and para-phenylene−ethylene oligomers and polymers have revealed two modes of bacteriocidal activity for Gram-positive and Gram-negative bacteria.[35] We have demonstrated a dark activity wherein association of the polymer or oligomer with the bacterial envelope leads to a breaching of the envelope and release of

cytoplasmic components (proteins and nucleic acids), leading to cell death. A second pathway for cell killing is activated with light being absorbed by the oligomer and polymer and activation of oxygen to produce singlet oxygen ($^1O_2$) and other ROS that promote damage by cross-linking of the cytoplasmic components.[34,36]

Herein, we present for the first time a full temporal photophysical characterization and antimicrobial activity for the cationic regio-regular P3HT-Im [∼60 polymer repeat units (PRU)] polymer with anionic sodium dodecyl sulfate (SDS) (Scheme 1), ranging from the sub-picosecond transient absorption dynamics to biocidal assays. Furthermore, steady-state structural characterization is utilized to derive the structure−function relationship for these P3HT-Im/SDS materials. The series of materials investigated consists of pure P3HT-Im, cationic (SDS to imidazole charge ratio <1), charge neutral (SDS to imidazole charge ratio = 1), and anionic (SDS to imidazole charge ratio >1) P3HT-Im/SDS materials. Dynamic light scattering (DLS), transmission electron microscopy (TEM), steady-state absorption, steady-state emission, time-resolved transient absorption, and biocidal assay were used to characterize the materials, biophysical, and antimicrobial properties of the materials. In total, this multidisciplinary study provides a direct correlation of the physical structure and electronic dynamics with biocidal activity.

■ RESULTS

The structures of the two major components and pictures of P3HT-Im/SDS material samples in the low-SDS concentration regime used in this study are shown in Scheme 1. The ∼60 PRU P3HT-Im and SDS are used at concentrations in water well below and above the critical micelle concentration (CMC) of 0.008 M (or 2.3 mg/mL) at room temperature (Table 1). Starting from the left, the photographs in Scheme 1 feature the pure well-solvated P3HT-Im polymer in aqueous solution followed by aliquot additions of SDS moving to the right at concentrations well below CMC. Notably, after one addition of SDS, the solution turns from a peach color to orange. Furthermore, addition of SDS changes the color to a solid purple that does not change upon further additions of SDS until SDS concentration reaches above CMC (Figure S1 in Supporting Information). At these high SDS concentrations, the color reverts back to the peach/yellow color (Figures S1 and S3). Note that the fourth solution from the left precipitated after 1 day of incubation. In this solution, the SDS to imidazole charge ratio is ∼1 and a coacervate (charge-balanced state) of complexes of the two components is formed. Due to lack of electrostatic repulsion, the small particles coalesce into larger particles and precipitate over time. All solutions outside of the charge-equivalent coacervate are stable for longer than 1 day without noticeable further changes.

The full range of P3HT-Im and SDS mixtures investigated in this work are outlined in Table 1. For ease of interpretation and further reference throughout the article, we define the solutions using the charge ratio of negatively charged SDS units to the number of positively charged imidazole units in the sample. Thus, for all cationic materials, the charge ratio is <1, and for anionic materials, the charge ratio is >1. During the course of our interrogation of these materials, it became clear that the behavior can be categorized into four charge ratio regimes: 0, <1, 1, and >1, exemplified by the 0, 0.33, 1, and 1.67 charge ratio samples (shaded in Table 1). Note that SDS

Table 1. Compositions and Charge Ratios for the Series of P3HT-Im/SDS Materials Investigated in This Study[a]

	Charge Ratio	(SDS) (µg/mL)	(P3HT-Im) (µg/mL)
1	0	0	50
2	0.16	10	50
3	0.33	20	50
4	0.668	40	50
5	0.99 (~ 1)	59.4	50
6	1.33	80	50
7	1.67	100	50
8	2.00	120	50
9	3.34	200	50
10	96	5.77×10^3	50
11	240	1.44×10^4	50

[a]Charge ratio is defined as the number of SDS charges divided by charges on P3HT-Im.

concentrations in these samples are far below its CMC. From henceforth, the main discussion focuses on properties of the four shaded samples in Table 1 with the full broader data set found in the Supporting Information. For completeness, we have collected limited DLS, steady-state, time-resolved, and biocidal activity results on the P3HT-Im (~60 RPU) with SDS concentrations above the CMC level. Detailed discussion for the above CMC samples are include in the Supporting Information (Figures S1−S10, S54).

DLS and TEM Characterization of P3HT-Im and P3HT-Im/SDS Materials in Aqueous Solution. Size distributions of P3HT-Im/SDS materials were measured by DLS and are shown in Figure 1. DLS data were measured in triplicate for each material.

The light scattering data indicate that the hydrodynamic diameter of a fresh sample of pure P3HT-Im (charge ratio = 0) is a little less than 10 nm with all measurements yielding an identical sharp monodispersed peak. Upon addition of SDS to

reach a charge ratio of 0.33, there is an increase in the diameter to between 10 and 100 nm. As inferred from the color change in the photographs (Scheme 1), the 0.33 charge ratio P3HT-Im/SDS material contains aggregated complexes with a broader distribution that formed quickly. The DLS measurements indicate that the sample at a charge ratio = 1 contains much larger particles than the other P3HT-Im/SDS materials, quickly forming aggregates about 1000 nm in diameter. Unlike all other materials, the charge neutral aggregates precipitate from solution over the course of multiple hours. Even though this is not evident from the photograph of the purple solution, the charge ratio 1.67 P3HT-Im/SDS material contains intermediate-size aggregates between the charge ratios 0.33 and 1 materials. Importantly, DLS measurements collected 1 day after sample preparation indicate that the sizes of both pure P3HT-Im and the charge ratios 0.33 and 1.67 P3HT-Im/SDS materials are stable in an aerated water environment.

We have examined the P3HT-Im/SDS aggregate materials by TEM, and representative images taken below the CMC of SDS are shown in Figure 2. The TEM images suggest that the P3HT-Im/SDS aggregates increase in size as the SDS/P3HT-Im ratio increases. For the lower SDS concentrations (charge

Figure 1. Intensity-weighted size distribution of P3HT-Im/SDS materials from DLS measurements for the 0 (black), 0.33 (red), 1 (green), and 1.67 (purple) charge ratio samples. All DLS measurements are made in triplicates with run 1 (solid line), run 2 (dashed line), and run 3 (dotted line).
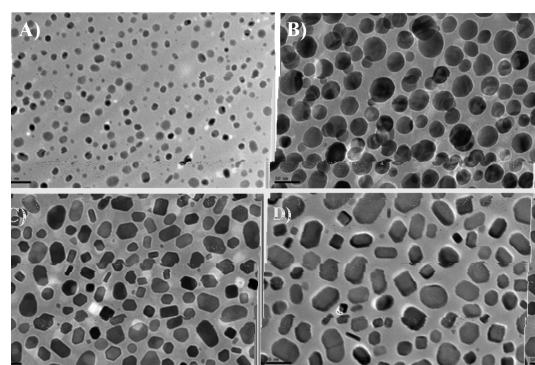
Figure 2. TEM images of aggregates obtained at P3HT-Im/SDS compositions below the CMC of SDS. The charge ratio 0.33 (A), charge ratio ~1 (B), and charge ratio 1.67 (C,D). The scale bar is 50 nm.

ratios 0.33 and 1, Figure 2A,B), the particles are roughly globular, but for a higher SDS concentration (charge ratios 1.67, Figure 2C,D), the particles appear crystalline, taking on a cuboid or prism-like shape. Similar to results from DLS, a wider range of particle sizes is observed with the higher SDS solution with particles ranging from ∼20 nm diameter to ∼80 nm. However, we note that ∼50 nm particle size of the charge ratio 1 material as visualized from the TEM image (Figure 2B) differs significantly from that obtained by DLS, where hydrodynamic diameter is about 1000 nm (Figure 1). As the coacervate is a highly dynamic solution where the particles coalesce and precipitate out of solution, the size difference could be caused by a difference in the incubation time of the samples, that is, the TEM sample is more fresh, artifacts of sample preparation (e.g., sample adsorption and the drying process during TEM grid preparation cause the particles to de-agglomerate), or the measurement method (e.g., DLS reports intensity average size distribution, where larger particles disproportionally contribute to scattering intensity). Significant particle overlap is also seen in the charge ratio = 1 material, which indicates conglomerate formation in solution.

Steady-State Photophysical Characterization of P3HT-Im and P3HT-Im/SDS Materials in Aqueous Solution. Steady-state absorption, excitation, emission, and synchronous emission for the pure P3HT-Im polymer (charge ratio = 0), cationic P3HT-Im/SDS material (charge ratio = 0.33), neutral P3HT-Im/SDS material (charge ratio = 1), and anionic P3HT-Im/SDS material (charge ratio = 1.67) are featured in Figure 3A−D. The pure P3HT-Im polymer shows
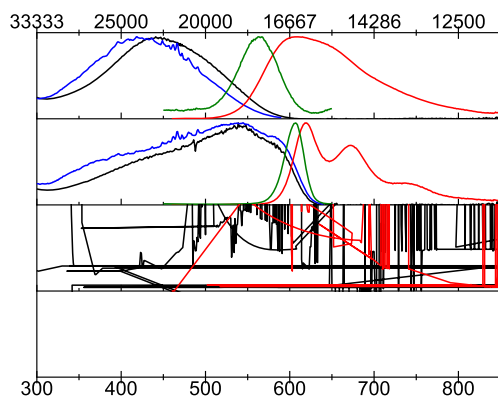
broad absorption and emission profiles from 300 to 600 nm (λ_{max} = 441 nm) and 500 to 850 nm (λ_{max} = 608 nm), respectively. The excitation profile of the P3HT-Im material is blue-shifted relative to its absorption spectrum with a maximum at 418 nm. Finally, the synchronous emission scan, which characterizes the $E^{0,0}$ state by analyzing the overlap between the absorption and emission,[37,38] is fit with a Gaussian profile to yield a maximum at 17820 cm^{-1} (561 nm) and a full width at half maximum (fwhm) of 1330 cm^{-1} (Figure S13).

Addition of SDS to the P3HT-Im polymer below the CMC results in large changes in the electronic absorption and emission spectra as seen in Figure 3. To our surprise, the positive P3HT-Im/SDS material (charge ratios <1), neutral

P3HT-Im/SDS material (charge ratio = 1), and negative P3HT-Im/SDS material (charge ratios >1) all exhibit remarkably similar absorption and emission spectra. All of the P3HT-Im/SDS material absorption and emission spectra show peaks at 588 and 548 nm, corresponding to the 0−0 and 0−1 absorption transitions, respectively, in aggregate structures. The P3HT-Im/SDS material exhibits 0−0, 0−1, and 0−2 emission transitions at 618, 672, and 735 nm, respectively. Unlike the pure P3HT-Im, the P3HT-Im/SDS material fluorescence excitation spectra do not feature a blue shift with the same 0−0 and 0−1 transitions as the absorption spectrum. Interestingly, when the P3HT-Im/SDS excitation and absorption spectra are normalized, a higher energy excitation shoulder (∼400 nm) is observed in the excitation spectrum but not in the absorption spectrum. The synchronous emission scan for the P3HT-Im/SDS material is fit with a Gaussian profile to yield a maximum at 16570 cm^{-1} (604 nm) and a FWHM of 760 cm^{-1} (Figures S15−S19). Finally, the fluorescence quantum yield (Φ_{fl}) was calculated from the emission data for P3HT-Im and P3HT-Im/SDS material using a ruthenium standard in water ([Ru(bpy)$_3$]Cl$_2$, Φ_{fl} = 0.045).[39] The Φ_{fl} for P3HT-Im is 0.096 and the P3HT-Im/SDS material Φ_{fl} ranges from 0.16 to 0.55 (Table 2). Again, only a representative fraction of P3HT-Im/SDS material spectra is depicted in Figure 3 with the full data set depicted in Figures S12 and S13.

The photostability of P3HT-Im and P3HT-Im/SDS materials has been investigated over the period of 1 day by monitoring their absorption under irradiated and dark-incubated conditions (Figures S55−S60). In general, all of the solutions in the dark maintain their integrity with small amounts of sample degradation. This stability is notable as many thiophene materials are typically stored under an inert atmosphere and in dark containers to avoid material degradation from photo-oxidation of the polymer backbone by locally generated $^1O_2$.[40−42] To this end, it is no surprise that significant degradation of the P3HT-Im is observed when the materials are continuously irradiated.

Time Resolved Photophysical Characterization of P3HT-Im and P3HT-Im/SDS Materials in Aqueous Solution. Depicted in Figure 4 are the absorption and nanosecond flash photolysis transient absorption spectra (collected at a time delay of 30 ns) for the pure P3HT-Im polymer and P3HT-Im/SDS materials at charge ratios of 0, 0.33, 1, and 1.67. The absorbance spectra featured in Figure 4A are the same absorbance spectra depicted in Figure 3 with the difference being that these spectra are not normalized. This highlights the difference in the absolute intensity of the signal and reinforces the lack of changes in spectral features between the different P3HT-Im/SDS materials. Shown in Figure 4B is the ns flash photolysis transient absorption spectrum of P3HT-Im, which exhibits an induced excited-state absorption from 422 to >850 nm and a ground-state depletion (bleach) from 300 to 422 nm with a minimum at 426 nm. The transient spectrum of P3HT-Im/SDS material at a charge ratio of 0.33 (Figure 4C) exhibits an excited-state absorption from 600 to 850 nm and a ground-state bleach from 330 to 600 nm. Specifically, three minima at 426, 552, and 584 nm are observed within the bleach region corresponding to the absorption maxima of the pure solvated material, aggregate 0−0, and 0−1 absorptions, respectively. The transient spectrum of P3HT-Im/SDS at a charge ratio of 1 (Figure 4D) exhibits two excited-state absorptions from 330 to 530 nm and 675 to >850

Table 2. Excited-State Lifetime (τ) and Fluorescence Quantum Yield (Φ_{fl}) Values Obtained from the fs Pump Probe and ns Flash Photolysis Experiments

	P3HT-Im	P3HT-Im/SDS charge ratio 0.33	P3HT-Im/SDS charge ratio 1	P3HT-Im/SDS charge ratio 1.67
τ_1 (ps)	0.5 ± 0.2		0.5 (fixed)[a]	0.29 ± 0.03
τ_2 (ps)	17 ± 3		6.3 ± 0.9	4.3 ± 0.5
τ_3 (ps)	290 ± 30		130 ± 10	120 ± 10
τ_4 (ns)		650 ± 120[b]	140 ± 50[c]	180 ± 10
τ_5 (ns)	13,670 ± 110	13580 ± 3390[b]	1240 ± 300[c]	
τ_{4or5} (ns,air)	2400 ± 50	2740 ± 120	1200 ± 100	250 ± 20
Φ_{fl}[d]	0.096	0.55	0.17	0.22

[a]Fixed time constant from average of t_1 single-wavelength kinetics. [b]Single-wavelength kinetics at 550 nm. [c]Single-wavelength kinetics at 470 nm. [d]We approximate the error of the Φ_{fl} to be within 10% of the value.
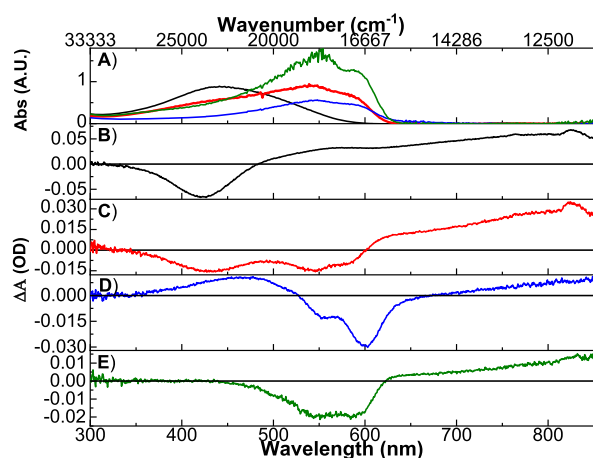
Figure 4. (A) Steady-state absorbance spectra of P3HT-Im (charge ratio = 0, black), cationic P3HT-Im/SDS (charge ratio = 0.33, red), neutral P3HT-Im/SDS (charge ratio = 1, blue), and anionic P3HT-Im/SDS (charge ratio = 1.67 green). Transient absorption spectra of P3HT-Im/SDS materials at charge ratios of 0 (B), 0.33 (C), 1 (D), and 1.67 (E); a 30 ns delay time was used for all measurements.

nm. The ground-state bleach of the charge-balanced P3HT-Im/SDS material extends from 530 to 675 with two minima at 555 and 602 nm. Finally, the transient spectrum of the anionic P3HT-Im/SDS material exhibits an excited-state absorption from 620 to >850 nm and a ground-state bleach from 430 to 620 nm. The fs pump probe spectra and decay dynamics leading to the ns flash photolysis data depicted in Figure 4 are found in Figures S21−S28. As the primary purpose for the time-resolved investigation of the P3HT-Im polymer and P3HT-Im/SDS materials is to probe the existence of long-lived triplet excited states from which ground-state $^3O_2$ can be sensitized to $^1O_2$, the fs pump probe spectra and decay dynamics, which characterize an early excited-state decay too fast for $^1O_2$ sensitization, are presented in the Supporting Information.

The time constants (τ) extracted from singular value decomposition global fitting of the fs pump probe and ns flash photolysis excited-state dynamics for the samples depicted in Figure 4 are summarized in Table 2. All excited-state dynamics are fit utilizing a multi-exponential function (eq S1 in the Supporting Information), where ΔOD is the difference of optical density (absorbance) at a given time delay, τ_p is the lifetime of the instrument response function limited by the laser excitation pulse, A is the weighted contribution of a fitted lifetime, τ_i is the fitted lifetime value,

and inf values are offset values in the case that ΔOD does not return back to 0.

$$\Delta OD = e^{-(t/\tau_\rho)} + \sum_i A_i e^{-(t/\tau_i)} + A_{inf} e^{-(t/\tau_{inf})},$$

$$\tau_\rho = (IRF/2\ln 2) \tag{1}$$

Single-wavelength kinetic fitting was also performed for multiple spectral features (Figures S30, S32, S34, S36, S38, and S40) and found to be overall internally consistent with the global kinetic fitting. Specifically, the fs pump probe transient absorption kinetics are fit to a triexponential function at which point, a quality residual was observed. Similarly, the ns flash photolysis was fit with a single exponential for the pure P3HT-Im (charge ratio = 0) and anionic P3HT-Im/SDS material (charge ratio = 1.67), while the cationic P3HT-Im/SDS material (charge ratio = 0.33) and neutral P3HT-Im/SDS material (charge ratio = 1) were fit with a bi-exponential function.

Biocidal Activities of the P3HT-Im/SDS Materials. As we have shown in a recent paper, various sized P3HT-Im polymers are effective antibacterial agents against a panel of pathogens.[35] Although these polymers have broad spectrum toxicity, we are interested in the possibility that the antimicrobial activity could be manipulated in a controlled manner by making nanoparticulate aggregates with SDS. Antimicrobial activities of the compounds were quantitatively determined from serial dilutions and counting of colony forming units (CFU) of *Escherichia coli* (*E. coli*) incubated with a P3HT-Im or P3HT-Im/SDS material for 30 min either in the dark ("dark") or under irradiation at 420 nm ("light"); results are shown in Figure 5. Here, log reduction in CFU is calculated using eq 2, where B is CFU remaining after treatment and A is CFU in the untreated control.

$$\text{Log CFU reduction} = \log\left(\frac{A}{B}\right) \tag{2}$$

To account for the effect of irradiation alone on *E. coli* viability, untreated controls were incubated both in the dark and under irradiation for 30 min at 420 nm. CFU from the appropriate control, either "dark" or "light", was used as value A in eq 2 to calculate log reduction of treated "dark" or "light" samples. As pure SDS has been reported to exhibit biocidal activity at high concentrations,[43−46] samples of *E. coli* treated with SDS alone were also prepared and incubated for 30 min either in the dark or under irradiation at 420 nm to determine if there is a competitive kill mechanism. Pictures of *E. coli* serial dilution plates for controls and treated samples are shown in
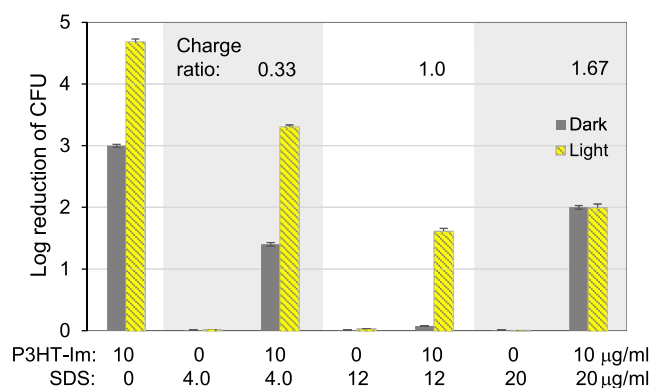
Figure 5. Log reduction of E. coli CFU incubated with different P3HT-Im/SDS materials for 30 min in the dark or under irradiation with 420 nm light. Concentrations of P3HT-Im and SDS for each sample are indicated below the plot, and charge ratios of the samples are shown at the top of the plot.

Figures S45−S53. Corresponding CFU counts from the plates are summarized in Tables S1−S7.

As shown in Figure 5, SDS alone over the range of concentrations investigated caused negligible cell death either in the dark or under irradiation. This is reasonable as SDS has been reported to exert toxicity at much higher concentrations, 1−2% (10−20 mg/mL) for E. coli[43] and 1.5−2% (15−20 mg/mL) for the Gram-negative salmonella enterica.[44] SDS has been shown to perturb the plasma membrane of E. Coli at a lower concentration of 0.05%, but the viability of growing cells is not affected.[45] Because SDS does not absorb light at 420 nm, it also did not have "light" antimicrobial activity (Figure 5).

Toxicities of the P4HT-Im/SDS materials tested were thus due to the polymer materials and not due to SDS or irradiation alone. The presence of 10 μg/mL pure P3HT-Im polymer results in 3.0 and 4.7 log kills under dark and irradiated incubation conditions, respectively. These log kill numbers are consistent with our previous studies using both CFU counting and flow cytometry techniques.[33,34,47] Addition of anionic SDS, which forms complexes with cationic P3HT-Im, at a charge ratio = 0.33, reduces dark and light log kills to 1.4 and 3.3, respectively. Furthermore, addition of SDS forms the neutral P3HT-Im/SDS material (charge ratio = 1), which quickly precipitates from solution. Dark antimicrobial activity of this coacervate is essentially abolished with a log kill value of 0.077. Under irradiation, the neutralized material has modest antimicrobial activity with a log kill of 1.6. Interestingly, at a charge ratio of 1.67, the net anionic material exhibits comparable dark and light activities with a log kill value of 2.0. We additionally evaluated antimicrobial activity at SDS concentrations close to and slightly above CMC (Figure S54). Results show that virtually no antimicrobial activity was observed against E. coli either in the dark or when irradiated with 420 nm light.

■ DISCUSSION

In order to understand the P3HT-Im polymer and P3HT-Im/SDS material biocidal activity, we have investigated the material characteristics that drives dark kill activity and the excited-state electronic structure that drives light kill activity. For organizational purposes, the physical and electronic structure discussion is presented together by material with the pure P3HT-Im polymer presented first and the P3HT-Im/
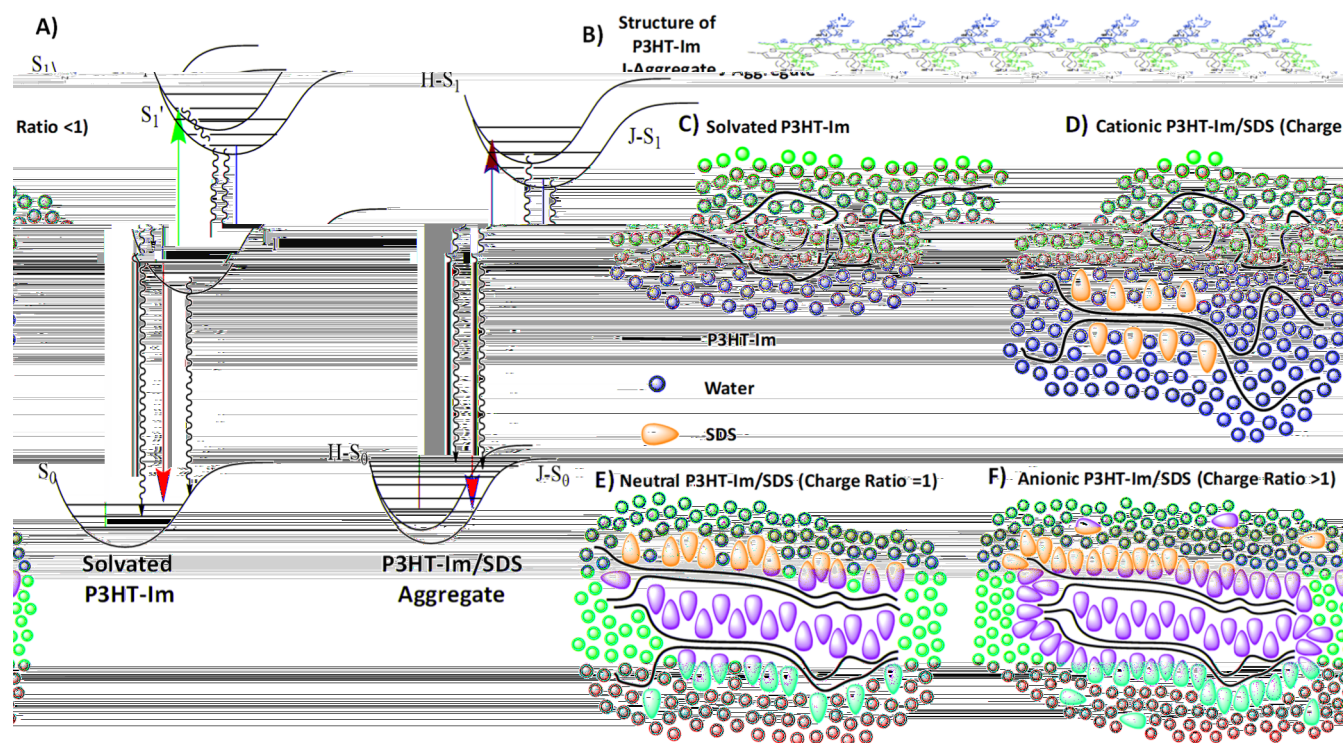
Figure 6. (A) Jablonski diagrams for solvated P3HT-Im and aggregated P3HT-Im/SDS materials. (B) Structure of the planer interchain J-type P3HT-Im aggregate. Note: H-type aggregates do not have a specific structure as the J-type but are defined as any other arrangement that is not a J-type. Possible structures of pure solvated P3HT-Im (C), cationic (charge ratio <1) (D), neutral (charge ratio = 1) (E), and anionic (charge ratio >1) (F) P3HT-Im/SDS materials.

SDS materials thereafter. A summary of the physical and electronic structure discussion is depicted in Figure 6. We conclude the discussion with the bioassay results predicted from the analysis of the physical and electronic structure.

The behavior of the pure P3HT-Im polymer in water is best described as a pristine well-solvated P3HT-Im single chain.[48] Note that this interpretation differs from our previous published work;[34] this study is primarily a new evaluation of the materials using steady-state absorption, emission, and DLS techniques and should be considered with literature examples. In our previous work, solvatochromic changes between the P3HT-Im polymer in methanol and water were interpreted as signs of aggregation. Results from this study show that they can be explained in terms of simple conformer changes. In general, broad featureless absorption (lack of vibronic progression) and emission (little or no vibronic progression) of all poly-thiophene materials are interpreted as "pristine" solvated polymers. This assignment is further strengthened by comparison of the shape of the emission and excitation profiles to earlier aggregation studies.[28,30,48] The broad, nearly featureless emission and slightly blue-shifted excitation of pure P3HT-Im (Figure 1A) have been ascribed in previous studies of poly(thiophene) materials to a distribution of emitting conformations (the excited state consisting of slightly different numbers of participating repeat units) from well-established excited-state torsion along a single-stranded polymer back-bone. Another contributor to the broad featureless behavior, characterized by the large FWHM observed in the synchro-nous experiment, is polydispersity of the polymer. In addition to polydispersity resulted from polymer synthesis, the size distribution of the P3HT materials measured by DLS can also vary based on the exact solvation environment of the sample. In this study, the pure P3HT-Im hydrodynamic diameter is determined to be <10 nm, which is reasonable for single-chain polymer strands. Such single polymer strands likely adopt an ensemble of conformations of differing degrees of self-folding, coiling, or solvent hydrogen bonding bridging of the P3HT-Im polymer and water. We note that the single-strand folding, coiling, or solvent bridging behavior is a solvatochromic behavior, which is different from polythiophene multi-chain polymer aggregation.

To assess the ROS generation capabilities of the pure P3HT-Im polymer, transient absorption spectroscopy with time delays ranging from fs to μs time scales was utilized. The femtosecond pump probe transient absorption of P3HT-Im (Figure S21) features the early time spectra and kinetics of the singlet excited state decay with eventual intersystem crossing (ISC) to the triplet state, depicting similar spectral features to the triplet state in Figure 4B. Multi-exponential kinetic fitting of the observed excited-state lifetimes yielded a sub-picosecond lifetime of 500 fs, picosecond lifetime of 17 ps, picosecond lifetime of 290 ps, and a microsecond lifetime of 13.67 μs (Figures S23 and S30). The sub-picosecond lifetime corresponding to the narrowing of the ground-state bleach region is consistent with previous reports of electron hole localization along the polymer backbone.[49,50] The second time constant of 17 ps is assigned to a combination of the polymer backbone torsional motions and excited-state electron hopping down the polymer backbone as previously demonstrated by fluorescence upconversion spectroscopy.[50,51] The 290 ps time constant is assigned to ISC to the thermally relaxed lowest triplet excited state as no other time components are observed in this experiment, and this excited state is reactive with oxygen

on longer time scales.[49,50] Importantly, the isosbestic points and spectral shifts seen in the early time spectra are indicative of sequential processes versus parallel reactions. The longest time constant (13.67 μs) is assigned to reverse ISC electron hole recombination occurring from the lowest triplet excited state to the singlet ground state.[49,52] Evidence for ROS ($^1O_2$ in this case) generation is found in the quenching of the triplet excited state lifetime from 13.67 to 2.4 μs upon aerating the deoxygenated sample. Furthermore, we have used 2,2,6,6-tetramethyl-4-piperidone (TEMPD) as an additional $^1O_2$ indicator detected by electron paramagnetic resonance (EPR) to monitor ROS generation (Figure S22). The clear increase in the radical signal of the TEMPD with pure P3HT-Im in comparison to the TEMPD standard is strong evidence for $^1O_2$ generation. The generation of other radical ROS molecules was monitored using a methyl violet indicator, which when mixed with P3HT-Im yielded no changes after irradiation (Figure S23). To our surprise, attempts to quantify the singlet oxygen generation by monitoring $^1O_2$ emission in water at ~1275 nm (Figure S20) were unsuccessful. We believe that this is due to water's ability to assist in the deactivation of triplet excited states, the short lifetime of $^1O_2$ in water (3 μs) in comparison to 30–300 μs for organic solvents, and the limitation of our instrumentation in detecting $^1O_2$ quantum yield less than 0.2.[53] This observation is partially corroborated by the observation of $^1O_2$ emission in DMSO (Figure S21).

The behavior of the cationic P3HT-Im/SDS material (charge ratio = 0.33) in water is somewhat different from that of the pure P3HT-Im polymer. The absorption, emission, and DLS data are internally consistent and clear in that addition of SDS to the P3HT-Im polymer induces multichain aggregation. The assignment of the H-type aggregate P3HT-Im/SDS material (Figure 3B) is made in the observation that the 0–0 transition is lower in intensity than the 0–1 transition of the absorption and excitation profile as defined by Spano et al..[28–30,54] Importantly, the emission spectra of the P3HT-Im/SDS materials are assigned to a J-type aggregate emission as the 0–0 transition has higher intensity than the 0–1 transition and not an H-type which is common in poly(thiophene) materials.[30,48] This discrepancy between the H-type absorb-ance and excitation with the J-type emission has been previously reported in careful aggregation studies where pure P3HT aggregates grown in a variety of solvent mixtures and temperature were observed to produce both H- and J-type structures in a single batch.[48] As the J aggregate structure is slightly lower in energy relative to the H aggregate, energy transfer to J aggregates and efficient non-radiative decay deactivates the H-type aggregate, resulting in dominant J emission for all species. The DLS and TEM images of the 0.33 charge ratio P3HT-IM/SDS material depict a large range of aggregate size and shapes, which makes it difficult to generate a single image of the material in solution. It is likely that a distribution of shapes exists ranging from the pure polymer (described above) to partially aggregated material with sections of the H aggregate structure and pure unaggregated structure (Figure 6).

Nanosecond flash photolysis transient absorption spectros-copy of the cationic P3HT-Im/SDS material (charge ratio = 0.33) agrees with the steady-state characterization depicting the solution as a mixture of the pure solvated polymer and aggregate material in the bleached region. Because of this mixture, fs pump probe transient absorption was not collected

due to the difficulty of deconvoluting early time components. However, longer-time scale transient absorption does not have this problem due to the drastic differences in lifetimes. The pure polymer lifetime of 13.67 μs is much longer than the 650 ns lifetime of the aggregate species. Importantly, aerating this cationic P3HT-Im/SDS aggregate material does not alter the 650 ns lifetime of the ground-state bleach and as expected shortens the lifetime of the pure P3HT-Im material to 2.7 μs. Based on the lack of lifetime changes in the presence of $^3O_2$ leads us to conclude that this aggregate P3HT-Im/SDS material (charge ratio = 0.33) does not generate a triplet excited state and thus will not generate ROS species. However, $^1O_2$ may still be generated from any un-aggregated P3HT-Im or partially aggregated P3HT-Im chains. Because of this, using ROS indicators in this material will not yield conclusive results as TEMPD will still react with $^1O_2$ generated by unaggregated and partially aggregated P3HT-Im in the sample. Furthermore, addition of SDS to P3HT-Im (charge ratio = 0.67) fully aggregates the remaining free P3HT-Im, as shown by ns spectroscopy. The P3HT-Im/SDS material (charge ratio = 0.67) does exhibit a low intensity, broad featureless positive absorption in the red lower energy region of the spectra, and a new positive absorption from 330 to 530 nm in the ns flash photolysis experiment. This low energy feature has been previously observed in neat aggregated polythiophene and polythiophene fullerene blended films to be a weak polaron absorption of relaxed polythiophene materials.[30,49,55,56] Two possibilities for the origin of the new absorption feature (Figure 4D) are a higher energy continuum of the polaron absorption, which is split by a higher-intensity ground-state bleach, or the presence of electronically isolated small segments of P3HT-Im energized by nearby aggregate excited states. We assign this new positive absorption (Figure 4D) to the latter explanation of electronically isolated small segments of P3HT-Im as further additions of SDS, which fully encapsulates all of the P3HT-Im, do not exhibit the same absorption feature. We describe this change in further detail below.

The behavior of the charge-neutral P3HT-Im/SDS material (charge ratio = 1) continues to evolve away from that of the pure P3HT-Im polymer. This coacervate P3HT-Im/SDS material initially forms round large aggregates (~1000 nm in hydrodynamic diameter) that coalesce and precipitate over time. Evidence for increased encapsulation of P3HT-Im is observed in the absorption spectra with the diminishment of the higher-energy shoulder at ~400 nm. To our surprise, the excitation profile, emission spectrum, and synchronous emission are identical to cationic P3HT-Im/SDS material (charge ratio = 0.33) for all charge ratios tested at the CMC. We will discuss more about the emission later.

Transient absorption spectroscopic data from the fs to μs time scale were also collected for the neutral P3HT-Im/SDS material (charge ratio = 1). The fs pump probe transient absorption spectra and kinetics for this P3HT-Im/SDS material are depicted in Figures S24−S26. These aggregate spectra are red-shifted from the pure polymer but have many similarities with the pure polymer including early time dynamics of electron localization (sup-picosecond), backbone torsion (~5 ps), and singlet relaxation (~120 ps). The differences start from the relaxation of the singlet excited state where no long-lived triplet state is populated. The pump probe spectra and kinetics clearly feature relaxation from the singlet excited state to low-intensity hot ground-state species with

broad polaron absorptions. These spectral and kinetic features are again identical to the neat aggregated polythiophene and polythiophene fullerene films.[30,49,55,56] Nanosecond flash photolysis transient absorption features continue from the fs pump probe experiments to show similar spectra to the cationic P3HT-Im/SDS material (charge ratio = 0.67). Notably, the positive absorption in the charge-equivalent material is less intense relative to the aggregate bleach and polaron NIR absorption in comparison to the cationic material with the 0−1 transition of the aggregate bleach vibronic structure being nicely resolved. We suspect that the higher-energy positive transient absorption signal is evidence of a small number of isolated P3HT-Im segments along the outer edge of the large P3HT-Im/SDS material aggregate. Finally, the absence of observed changes in the 140 ns or 1.2 μs lifetimes in the presence of $^3O_2$ for the P3HT-Im/SDS material (charge ratio = 1) does not support the presence of excited-state triplets or generation of ROS.

The behavior of the anionic P3HT-Im/SDS material (charge ratio from 1 to the CMC limit) is closest to resemble neat aggregated polythiophene materials. Transient absorption spectroscopy from the fs to μs time scale was collected for the anionic P3HT-Im/SDS material (charge ratio = 1.67). The fs pump probe transient absorption spectra and kinetics for this P3HT-Im/SDS material are depicted in Figures S27−S29. These aggregate spectra show similarities with the pure polymer and neutral aggregate (charge ratio = 1), including early electron localization (sup-picosecond), backbone torsion (~5 ps), and singlet relaxation (~120 ps). Again, no triplet spectral signature is observed in the anionic P3HT-Im/SDS material (charge ratio = 1.67), and the ns flash photolysis spectra of this material are different from those of the cationic and neutral aggregate in the lack of a higher-energy induced absorption peak. Moreover, unlike the other aggregate materials, the bleach region has a well-defined H-aggregate structure. We interpret this change to mean one of two possibilities, either that the remaining electronically isolated P3HT-Im segment population is now encapsulated by SDS or that continual increase in SDS beyond the charge equivalent point enables a new non-radiative pathway for deactivation of the isolated P3HT-Im segment excited state. Based on the lack of significant kinetic changes between the charge neutral and anionic aggregate P3HT-Im/SDS aggregates, we believe that the first case is more likely. Finally, aerating the anionic aggregate P3HT-Im/SDS material (charge ratio = 1.67) does not alter the 180 ns lifetimes, thus again arguing against the formation of excited-state triplets or generation of ROS.

The behavior of the P3HT-Im/SDS material near and well above the SDS CMC level does not resemble that of the other P3HT-Im/SDS materials or the pure P3HT-Im polymer. Although the color of the P3HT-Im/SDS material at CMC solution nearly reverts to that of the P3HT-Im polymer, femtosecond pump probe transient absorption response of the material has noticeable differences. Based on our experience with P3HT materials, we compared the P3HT-Im/SDS material at CMC spectroscopic signatures with that of a P3HT-Im oligomer to yield a match. This means that the P3HT-Im/SDS material at CMC behaves as a series of short P3HT-Im chains when in an SDS micelle rather than a pure polymer. This includes the observation that the P3HT-Im/SDS material at CMC regains the presence of a long lived triplet state from which ROS generation may be possible. A full

discussion of the P3HT-Im/SDS material at CMC dynamics is given in the Supporting Information.

The sum total of our physical and electronic structure characterization of the P3HT-Im/SDS material is contained in Figure 6 that features a Jablonski-type diagram (depicting the photophysics) and suggested structures for the P3HT-Im/SDS materials at different SDS concentrations. The important takeaways from the Jablonski-type diagrams (Figure 6A) are that the pure polymer fluorescence and ISC occur from a displaced singlet excited state while with ROS generated from the long-lived triplet state. For the polymer aggregate material, all fluorescence occurs from a sub population of J-type (not the predominate H-type) aggregates with no triplet state formation. This observation is notable as polymer materials in biological environments are typically analyzed by luminescence spectroscopy which in this example will not report on the majority of the solution chemistry dominated by H-type aggregate materials. Notably, conflict between the initial observation of invariant J-type emission (excitation, emission, and synchronous emission) and clear changes in the H-type absorption (DLS, TEM, absorption, and time-resolved spectroscopy) for all of the aggregate species surprised us until we realized that the J-aggregate emission originates from a small minor population species, thus not reporting on the majority of the solution chemistry dominated by H-type aggregates.

We find this revelation to be an important lesson for the greater bio-inorganic community as many studies rely exclusively on photoluminescence measurements without much concern about the nature of the emitting chromophore. Furthermore, depicted in Figure 6B−F are the proposed structures of the pristine J-type P3HT aggregate and the soft aggregate P3HT-Im/SDS materials in water. It is important for us to revisit the long slip stack structure of the J-type aggregate (Figure 6B) because all other types of weakly coupled aggregates that are not this J structure are defined as the H-type aggregate.[28,54,56] Shown in Figure 6C is the proposed structure of the pristine solvated P3HT-Im polymer in water. Again, we acknowledge the likelihood that solvatochromic interactions such as self-folding and water-mediated hydrogen bonding along single polymer strands are occurring but note that these effects are not the same as multichain polymer aggregation. Figure 6D depicts the proposed structure of the cationic P3HT-Im/SDS material (charge ratio <1), where we believe that partial multichain aggregation of the P3HT-Im polymer occurs alongside the residual unaggregated polymer. In the neutral P3HT-Im/SDS material (charge ratio = 1), SDS likely binds to the entire surface of the polymer. Notably, we make an attempt to depict that charge neutral simply means that the number of SDS to positive imidazole units is balanced, which is not the same as every imidazole unit has an adjacent SDS molecule thus resulting in some surface areas have more SDS coverage than others. Finally, the anionic P3HT-Im/SDS material (charge ratio >1) is composed of aggregates where all of the P3HT-Im polymer surface is likely covered with SDS. We believe that this high degree of SDS coverage plays an important role in the anionic P3HT-Im/SDS material's biocidal activity which is elaborated below.

In view of the results from the physical and electronic structural investigations of the pure P3HT-Im polymer and the aggregated P3HT-Im/SDS materials, the results of the biocidal toxicity of the P3HT-Im SDS material are surprising. Our previous work focusing on the biocidal activity pure P3HT-Im

in the presence of different bacteria (*S. aureus*, *S. epidermidis*, *P. aeruginosa*, and *E. coli*) showed that biocidal activity in the presence of light was due to ROS ($^1O_2$ generation from a triplet excited state of P3HT-Im) as cross-linking of components found in the cytoplasm were observed.[33] The biocidal activity under dark conditions however occurred via binding between the P3HT-Im polymer and bacterial envelope. Images of the bacteria post treatment with P3HT-Im under dark conditions indicate that the cationic polymer binding to the anionic bacterial envelope cause the bacterial envelope to rupture and release its contents into the buffer polymer mixture.[33] From these findings, we predicted that the P3HT-Im/SDS material would exhibit less light killing activity as the SDS concentration is increased due to the lack of triplet excited state formation. We further predict a decrease in the dark killing of P3HT-Im/SDS material with increasing SDS concentrations as complexation of SDS with the cationic P3HT-Im reduces its charge and, thereby, binding to *E. coli*. When charge ratio is >1, electrostatic repulsion between the anionic P3HT-Im/SDS material and anionic bacterial envelope is expected and as such no dark antimicrobial activity is anticipated.

The antimicrobial activity results shown in Figure 5 are mostly consistent with our predictions with a few surprises. With a sub-stoichiometric ratio of SDS added (charge ratio = 0.33), the cationic P3HT-Im/SDS material exhibits a reduced log reduction of 1.4 under dark incubation compared to pure P3HT-Im of 3.0. We rationalize this result by first noting that at the 0.33 charge ratio, there is still significant free P3HT-Im present in the sample that can bind to and induce toxicity to *E. coli* through disruption of the bacterial envelope. Consistent with previously published results,[35] irradiation of the pure P3HT-Im induced an additional 1.7 log reduction of CFU. Moreover, treating *E. coli* with P3HT-Im for only 10 min yielded an identical log reduction to the 30 min treatment, thus showing that the pure P3HT-Im material ROS generation is very efficient at triggering *E. coli* death.[35] Therefore, the dark- and light-activated antimicrobial activities, albeit suppressed compared to pure P3HT-Im, of the cationic P3HT-Im/SDS material (charge ratio 0.33) can be attributed to the free (or unaggregated) P3HT-Im polymer. The light killing activity results from $^1O_2$ formation from the unaggregated P3HT-Im while the suppression of the dark kill activity is attributed to SDS diminishing the net positive charge of the P3HT-Im, resulting in weaker binding, and thereby less disruption, to the *E. coli* bacterial envelope.

We ascribe the lack of efficient dark biocidal activity in the presence of the charge-neutral P3HT-Im/SDS material (charge ratio = 1) (Figure 5) to a combination of factors. First, P3HT-Im/SDS complexes in this coacervate material are not colloidally stable and precipitate over time. Complete neutralization of the cationic charges on the P3HT-Im polymer and precipitation remove the active P3HT-Im polymer from solution to interact with *E. coli* and exert antimicrobial activity. The polymer bound SDS to prevent fast association of the P3HT-Im polymer to the *E. coli* bacterial envelope. Although it is possible for SDS to exchange with other anions in the bacterial envelope, we believe this process to be slow relative to the timescale of the experiment as it lacks a large driving force. Our transient absorption measurements show that no accessible triplet state is detected. However, a log reduction of 1.6 is still observed. Unlike the charge ratio 0.33 material where free P3HT-Im remains, the light killing in the charge

ratio 1 material could be due to small segments of the polymer chain that have less SDS coverage.

Increasing SDS concentration further to a charge ratio of 1.67 yields an anionic P3HT-Im/SDS material. To our surprise, this weakly anionic material reproducibly exhibits comparable log reductions of 2.0 both in the dark and under irradiation. A thorough literature search revealed a number of biocidal studies featuring anionic coated aggregates that are able to trigger fungal or bacterial death by binding to select positively charged sites on the predominantly anionic outer envelope.[57−59] These investigations concluded that while an electrostatic repulsion does exist between the bacterial envelope and the anionic aggregates, this repulsion leads to slower kinetics for aggregate binding and lower antimicrobial activity over a limited time window, but the binding event itself is driven by the components of the bacterial envelope and not simply the bacterial envelope net charge.[59] Once bound, the anionic aggregates are able to disrupt numerous cell processes depending on the exact binding site. The anionic P3HT-Im/ SDS complexes formed in this material are dynamic. Binding of the complexes to cationic components to the bacterial envelope places the highly active P3HT-Im polymer close to the bacterial envelope, which can be released to exert toxicity when SDS binds instead to components in the bacterial envelope. Irradiation of the charge ratio 1.67 material did not cause additional killing of E. coli. This result is not surprising in view of the time-resolved spectroscopic investigation in the absence of bacteria which did not detect the formation of an excited triplet state from which ROS could be efficiently generated. The lack of ns lifetime changes between a de-aerated and aerated sample indicates that no ROS formation is taking place from light excitation. Thus, irradiation did not cause any more toxicity toward E. coli in addition to the 2 logs of reduction due to dark activity.

We note that increasing SDS concentrations significantly to half and slightly above its CMC to charge ratios of 96 and 240 (Table 1), respectively, abolished both dark and light activities of P3HT-Im (Figure S54). At these high SDS concentrations, P3HT-Im is completely sequestered by SDS assemblies and behave like solubilized monomeric oligomers as indicated by the spectroscopic results present above. Although the spectroscopic results identify a long-lived triplet excited state which could generate ROS, the constrained P3HT-Im polymer within the SDS is unable to exert any toxicity toward E. coli.

■ CONCLUSIONS

In this study, we have characterized the size, shape, photophysical properties, and biocidal activities for a novel series of soft aggregate P3HT-Im/SDS nanomaterials. P3HT-Im is a highly effective antimicrobial polymer, exhibiting >4 log reductions of E. coli viability by a combination of dark and light-activated pathways. Also, unlike other methods currently pursued for disinfection of drug-resistant bacteria, these materials have been shown to have low toxicity to mammalian cells and they also do not produce toxic degradation products such as many inorganic antimicrobials, which have heavy metal degradation products. We show here that we can control the antimicrobial activities of P3HT-Im by complexation with an oppositely charged detergent SDS. Addition of SDS yielded

Eva Chi − Center for Biomedical Engineering and Department of Chemical and Biological Engineering, University of New Mexico, Albuquerque, New Mexico 87131, United States; ⊙ orcid.org/0000-0001-7448-9943; Email: evachi@unm.edu

David G. Whitten − Department of Chemistry and Chemical Biology, Center for Biomedical Engineering, and Department of Chemical and Biological Engineering, University of New Mexico, Albuquerque, New Mexico 87131, United States; ⊙ orcid.org/0000-0002-6305-9494; Email: whitten@unm.edu

Authors

Jianzhong Yang − Center for Biomedical Engineering and Department of Chemical and Biological Engineering, University of New Mexico, Albuquerque, New Mexico 87131, United States

Fahimeh Maghsoodi − Nanoscience and Microsystems Engineering Graduate Program, University of New Mexico, Albuquerque, New Mexico 87131, United States

Andrea Scheberl − Department of Nanobiotechnology, University of Natural Resources and Life Sciences, Vienna A-1190, Austria

Samuel M. Greer − Los Alamos National Laboratory (LANL), Los Alamos, New Mexico 87545, United States; ⊙ orcid.org/0000-0001-8225-3252

Mohammed I. Khalil − Center for Biomedical Engineering and Department of Chemical and Biological Engineering, University of New Mexico, Albuquerque, New Mexico 87131, United States

Edward Strach − Center for Biomedical Engineering and Department of Chemical and Biological Engineering, University of New Mexico, Albuquerque, New Mexico 87131, United States

Dylan Brown − Center for Biomedical Engineering and Department of Chemical and Biological Engineering, University of New Mexico, Albuquerque, New Mexico 87131, United States

Complete contact information is available at:
https://pubs.acs.org/10.1021/acsami.1c18553

Author Contributions

Conception and design: M.Y.L., J.Y., J.J.R., and D.G.W. Experimental work: M.Y.L. (spectroscopic characterizations), J.Y. (P3HT-Im synthesis and TEM), F.M. (antimicrobial activity and stability), A.S. (DLS), and S.M.G. (EPR). M.K., E.S., and D.B. contributed during the early phase of the study and prepared samples and carried out preliminary antimicrobial activity assays. Data interpretation: M.Y.L., S.M.G., E.C., and D.G.W. Article preparation: M.Y.L. Article revision: M.Y.L., F. M., B.W.S., E.R., J.J.R., E.C., and D.G.W.

Notes

The authors declare the following competing financial interest(s): J.Y. was funded in part from BioSafe, a startup company in which DGW is a founder and shareholder.

■ REFERENCES

(1) Antibiotic Resistance Threats in the United States. 2019, https://stacks.cdc.gov/view/cdc/82532: Atlanta, GA, 2019.

(2) Haque, M.; Sartelli, M.; McKimm, J.; Abu Bakar, M. B. Health care-associated infections—an overview. Infect. Drug Resist. 2018, 11, 2321−2333.

(3) Antimicrobial Resistance: Global Report on Surveillance. 2014, https://www.who.int/drugresistance/documents/surveillancereport/en/2014.

(4) Egorov, A. M.; Ulyashova, M. M.; Rubtsova, M. Y. Bacterial Enzymes and Antibiotic Resistance. Acta Fac. Rerum Nat. Univ. Comenianae, Form. Prot. Nat. 2018, 10, 33−48.

(5) Wright, G. Bacterial Resistance to Antibiotics: Enzymatic Degradation and Modification. Adv. Drug Deliv. Rev. 2005, 57, 1451−1470.

(6) Fleitas Martínez, O.; Cardoso, M. H.; Ribeiro, S. M.; Franco, O. L. Recent Advances in Anti-virulence Therapeutic Strategies With a Focus on Dismantling Bacterial Membrane Microdomains, Toxin Neutralization, Quorum-Sensing Interference and Biofilm Inhibition. Front. Cell. Infect. Microbiol. 2019, 9, 74.

(7) Tagliabue, A.; Rappuoli, R. Changing Priorities in Vaccinology: Antibiotic Resistance Moving to the Top. Front. Immunol. 2018, 9, 1068.

(8) Garcia-Mayea, Y.; Mir, C.; Masson, F.; Paciucci, R.; Lleonart, M. E. Insights into New Mechanisms and Models of Cancer Stem Cell Multidrug Resistance. Semin. Cancer Biol. 2020, 60, 166−180.

(9) Pang, Z.; Raudonis, R.; Glick, B. R.; Lin, T.-J.; Cheng, Z. Antibiotic Resistance in Pseudomonas Aeruginosa: Mechanisms and Alternative Therapeutic Strategies. Biotechnol. Adv. 2019, 37, 177−192.

(10) Du, D.; Wang-Kan, X.; Neuberger, A.; van Veen, H. W.; Piddock, L. J. V.; Luisi, B. F.; Luisi, B. F. Multidrug Efflux Pumps: Structure, Function and Regulation. Nat. Rev. Microbiol. 2018, 16, 523−539.

(11) Li, J.; Zhong, W.; Zhang, K.; Wang, D.; Hu, J.; Chan-Park, M. B. Biguanide-Derived Polymeric Nanoparticles Kill MRSA Biofilm and Suppress Infection In Vivo. ACS Appl. Mater. Interfaces 2020, 12, 21231−21241.

(12) Zhang, K.; Du, Y.; Si, Z.; Liu, Y.; Turvey, M. E.; Raju, C.; Keogh, D.; Ruan, L.; Jothy, S. L.; Reghu, S.; Marimuthu, K.; De, P. P.; Ng, O. T.; Mediavilla, J. R.; Kreiswirth, B. N.; Chi, Y. R.; Ren, J.; Tam, K. C.; Liu, X.-W.; Duan, H.; Zhu, Y.; Mu, Y.; Hammond, P. T.; Bazan, G. C.; Pethe, K.; Chan-Park, M. B. Enantiomeric Glycosylated Cationic Block Co-Beta-Peptides Eradicate Staphylococcus Aureus Biofilms and Antibiotic-Tolerant Persisters. Nat. Commun. 2019, 10, 4792.

(13) Yeo, C. K.; Vikhe, Y. S.; Li, P.; Guo, Z.; Greenberg, P.; Duan, H.; Tan, N. S.; Chan-Park, M. B. Hydrogel Effects Rapid Biofilm Debridement with ex situ Contact-Kill to Eliminate Multidrug Resistant Bacteria in vivo. ACS Appl. Mater. Interfaces 2018, 10, 20356−20367.

(14) Cieplik, F.; Deng, D.; Crielaard, W.; Buchalla, W.; Hellwig, E.; Al-Ahmad, A.; Maisch, T. Antimicrobial photodynamic therapy - what we know and what we don't. Crit. Rev. Microbiol. 2018, 44, 571−589.

(15) Hamblin, M. R. Antimicrobial Photodynamic Inactivation: a Bright New Technique to Kill Resistant Microbes. Curr. Opin. Microbiol. 2016, 33, 67−73.

(16) Vatansever, F.; de Melo, W. C. M. A.; Avci, P.; Vecchio, D.; Sadasivam, M.; Gupta, A.; Chandran, R.; Karimi, M.; Parizotto, N. A.; Yin, R.; Tegos, G. P.; Hamblin, M. R. Antimicrobial strategies centered around reactive oxygen species - bactericidal antibiotics, photodynamic therapy, and beyond. FEMS Microbiol. Rev. 2013, 37, 955−989.

(17) van Dijk, B.; Lemans, J. V. C.; Hoogendoorn, R. M.; Dadachova, E.; de Klerk, J. M. H.; Vogely, H. C.; Weinans, H.; Lam, M. G. E. H.; van der Wal, B. C. H. Treating Infections with

Ionizing Radiation: a Historical Perspective and Emerging Techniques. Antimicrob. Resist. Infect. Control 2020, 9, 121.

(18) Abergel, R.; An, D.; Lakes, A.; Deblonde, G.; Rees, J.; Gauny, S.; Sridharan, D. Targeted Radionuclide Therapy: The Promise of Short-Lived Alpha-Emitting Actinides. Abstr. Pap. Am. Chem. Soc. 2019, 257.

(19) Kessel, D. Photodynamic Therapy: A Brief History. J. Clin. Med. 2019, 8, 1581.

(20) Aljarrah, K.; Al-Akhras, M.-A.; Al-Khalili, D. J.; Ababneh, Z. The Feasibility of Using Saffron to Reduce the Photosensitivity Reaction of Selected Photosensitizers Using Red Blood Cells and StaphylococcusAureus Bacteria as Targets. Photodiagnosis Photodyn. Ther. 2020, 29, 101590.

(21) Traina, C. A.; Bakus, R. C.; Bazan, G. C. Design and Synthesis of Monofunctionalized, Water-Soluble Conjugated Polymers for Biosensing and Imaging Applications. J. Am. Chem. Soc. 2011, 133, 12600−12607.

(22) Feng, X.; Liu, L.; Wang, S.; Zhu, D. Water-Soluble Fluorescent Conjugated Polymers and Their Interactions with Biomacromolecules for Sensitive Biosensors. Chem. Soc. Rev. 2010, 39, 2411−2419.

(23) Yuan, H.; Wang, B.; Lv, F.; Liu, L.; Wang, S. Conjugated-Polymer-Based Energy-Transfer Systems for Antimicrobial and Anticancer Applications. Adv. Mater. 2014, 26, 6978−6982.

(24) Toba, M.; Nakashima, T.; Kawai, T. Phenyleneethynylene- and Thienyleneethynylene-Based π-Conjugated Polymers with Imidazolium Units in the Main Chain. Macromolecules 2009, 42, 8068−8075.

(25) Knaapila, M.; Evans, R. C.; Garamus, V. M.; Almásy, L.; Székely, N. K.; Gutacker, A.; Scherf, U.; Burrows, H. D. Structure and "Surfactochromic" Properties of Conjugated Polyelectrolyte (CPE): Surfactant Complexes between a Cationic Polythiophene and SDS in Water. Langmuir 2010, 26, 15634−15643.

(26) Li, F.; Yager, K. G.; Dawson, N. M.; Yang, J.; Malloy, K. J.; Qin, Y. Complementary Hydrogen Bonding and Block Copolymer Self-Assembly in Cooperation toward Stable Solar Cells with Tunable Morphologies. Macromolecules 2013, 46, 9021−9031.

(27) Brambilla, L.; Tommasini, M.; Botiz, I.; Rahimi, K.; Agumba, J. O.; Stingelin, N.; Zerbi, G. Regio-Regular Oligo and Poly(3-hexyl thiophene): Precise Structural Markers from the Vibrational Spectra of Oligomer Single Crystals. Macromolecules 2014, 47, 6730−6739.

(28) Niles, E. T.; Roehling, J. D.; Yamagata, H.; Wise, A. J.; Spano, F. C.; Moulé, A. J.; Grey, J. K. J-Aggregate Behavior in Poly-3-hexylthiophene Nanofibers. J. Phys. Chem. Lett. 2012, 3, 259−263.

(29) Spano, F. C. The Spectral Signatures of Frenkel Polarons in H- and J-Aggregates. Acc. Chem. Res. 2010, 43, 429−439.

(30) Thomas, A. K.; Garcia, J. A.; Ulibarri-Sanchez, J.; Gao, J.; Grey, J. K. High Intrachain Order Promotes Triplet Formation from Recombination of Long-Lived Polarons in Poly(3-hexylthiophene) J-Aggregate Nanofibers. ACS Nano 2014, 8, 10559−10568.

(31) Gangopadhyay, P.; Voorakaranam, R.; Lopez-Santiago, A.; Foerier, S.; Thomas, J.; Norwood, R. A.; Persoons, A.; Peyghambarian, N. Faraday Rotation Measurements on Thin Films of Regioregular Alkyl-Substituted Polythiophene Derivatives. J. Phys. Chem. C 2008, 112, 8032−8037.

(32) Zhang, Z.; Zong, X.; Sun, Z.; Qin, Y. Impact of Side-Chain Extension on Physical and Electronic Properties of Cross-Conjugated Poly(thienylene vinylene)s (PTVs). Polymer 2019, 166, 115−122.

(33) Brown, D. M.; Yang, J.; Strach, E. W.; Khalil, M. I.; Whitten, D. G. Size and Substitution Effect on Antimicrobial Activity of Polythiophene Polyelectrolyte Derivatives Under Photolysis and Dark Conditions. Photochem. Photobiol. 2018, 94, 1116−1123.

(34) Huang, Y.; Pappas, H. C.; Zhang, L.; Wang, S.; Cai, R.; Tan, W.; Wang, S.; Whitten, D. G.; Schanze, K. S. Selective Imaging and Inactivation of Bacteria over Mammalian Cells by Imidazolium-Substituted Polythiophene. Chem. Mater. 2017, 29, 6389−6395.

(35) Scheberl, A.; Khalil, M. L.; Maghsoodi, F.; Strach, E. W.; Yang, J.; Chi, E. Y.; Schanze, K. S.; Reimhult, E.; Whitten, D. G. Quantitative Determination of Dark and Light-Activated Antimicrobial Activity of Poly(Phenylene Ethynylene), Polythiophene, and Oligo(Phenylene Ethynylene) Electrolytes. ACS Appl. Mater. Interfaces 2020, 12, 21322−21329.

(36) Wang, Y.; Schanze, K. S.; Chi, E. Y.; Whitten, D. G. When Worlds Collide: Interactions at the Interface between Biological Systems and Synthetic Cationic Conjugated Polyelectrolytes and Oligomers. Langmuir 2013, 29, 10635−10647.

(37) Vo-Dinh, T. Synchronous Luminescence Spectroscopy: Methodology and Applicability. Appl. Spectrosc. 1982, 36, 576−581.

(38) Vo-Dinh, T. Multicomponent Analysis by Synchronous Luminescence Spectrometry. Anal. Chem. 1978, 50, 396−401.

(39) Marco Montalti, A. C.; Prodi, L. Teresa Gandolfi Handbook of Photochemistry. In Handbook of Photochemistry, 3rd ed; CRC Press, 2006; Chapter 5, pp 377−420.

(40) Cook, S.; Furube, A.; Katoh, R. Matter of Minutes Degradation of Poly(3-hexylthiophene) Under Illumination in Air. J. Mater. Chem. 2012, 22, 4282−4289.

(41) Ohta, H.; Koizumi, H. Mechanisms of Photo-Induced Degradation of Polythiophene Derivatives: Re-examination of the Role of Singlet Oxygen. Polym. Bull. 2017, 74, 2319−2330.

(42) Sivula, K.; Luscombe, C. K.; Thompson, B. C.; Fréchet, J. M. J. Enhancing the Thermal Stability of Polythiophene:Fullerene Solar Cells by Decreasing Effective Polymer Regioregularity. J. Am. Chem. Soc. 2006, 128, 13988−13989.

(43) Elramady, M. G.; Aly, S. S.; Rossitto, P. V.; Crook, J. A.; Cullor, J. S. Synergistic Effects of Lactic Acid and Sodium Dodecyl Sulfate to Decontaminate Escherichia coli O157:H7 on Cattle Hide Sections. Foodborne Pathog. Dis. 2013, 10, 661−663.

(44) Zhao, T.; Zhao, P.; Doyle, M. P. Inactivation of Salmonella and Escherichia coli O157:H7 on Lettuce and Poultry Skin by Combinations of Levulinic Acid and Sodium Dodecyl Sulfate. J. Food Prot. 2009, 72, 928−936.

(45) Woldringh, C. L.; van Iterson, W. Effects of Treatment with Sodium Dodecyl Sulfate on the Ultrastructure of Escherichia Coli. J. Bacteriol. Res. 1972, 111, 801−813.

(46) Li, L.; Molin, S.; Yang, L.; Ndoni, S. Sodium Dodecyl Sulfate (SDS)-Loaded Nanoporous Polymer as Anti-Biofilm Surface Coating Material. Int. J. Mol. Sci. 2013, 14, 3050.

(47) Donabedian, P. L.; Creyer, M. N.; Monge, F. A.; Schanze, K. S.; Chi, E. Y.; Whitten, D. G. Detergent-Induced Self-Assembly and Controllable Photosensitizer Activity of Diester Phenylene Ethynylenes. Proc. Natl. Acad. Sci. U.S.A. 2017, 114, 7278−7282.

(48) Thomas, A. K.; Brown, H. A.; Datko, B. D.; Garcia-Galvez, J. A.; Grey, J. K. Interchain Charge-Transfer States Mediate Triplet Formation in Purified Conjugated Polymer Aggregates. J. Phys. Chem. C 2016, 120, 23230−23238.

(49) Banerji, N.; Seifter, J.; Wang, M.; Vauthey, E.; Wudl, F.; Heeger, A. J. Ultrafast Spectroscopic Investigation of a Fullerene Poly(3-hexylthiophene) Dyad. Phys. Rev. B: Condens. Matter Mater. Phys. 2011, 84, 075206.

(50) Banerji, N.; Cowan, S.; Vauthey, E.; Heeger, A. J. Ultrafast Relaxation of the Poly(3-hexylthiophene) Emission Spectrum. J. Phys. Chem. C 2011, 115, 9726−9739.

(51) Hwang, I.; Scholes, G. D. Electronic Energy Transfer and Quantum-Coherence in π-Conjugated Polymers. Chem. Mater. 2011, 23, 610−620.

(52) Burrows, H. D.; Miguel, M. d. G.; Monkman, A. P.; Hamblett, I.; Navaratnam, S. Transient Absorption Spectra of Triplet States and Charge Carriers of Conjugated Polymers. J. Mol. Struct. 2001, 563−564, 41−50.

(53) Livshits, M. Y.; He, W.; Zhang, Z.; Qin, Y.; Rack, J. J. Triplet Excited-State Energetics and Dynamics in Molecular "Roller Wheels". J. Phys. Chem. C 2019, 123, 16556−16564.

(54) Hestand, N. J.; Spano, F. C. Expanded Theory of H- and J-Molecular Aggregates: The Effects of Vibronic Coupling and Intermolecular Charge Transfer. Chem. Rev. 2018, 118, 7069−7163.

(55) Ferreira, B.; da Silva, P. F.; Seixas de Melo, J. S.; Pina, J.; Maçanita, A. Excited-State Dynamics and Self-Organization of Poly(3-hexylthiophene) (P3HT) in Solution and Thin Films. J. Phys. Chem. B 2012, 116, 2347−2355.

L

(56) Ghosh, R.; Spano, F. C. Excitons and Polarons in Organic Materials. *Acc. Chem. Res.* **2020**, *53*, 2201−2211.

(57) Pillai, P. P.; Kowalczyk, B.; Kandere-Grzybowska, K.; Borkowska, M.; Grzybowski, B. A. Engineering Gram Selectivity of Mixed-Charge Gold Nanoparticles by Tuning the Balance of Surface Charges. *Angew. Chem., Int. Ed.* **2016**, *55*, 8610−8614.

(58) Lyden, A.; Lombardi, L.; Sire, W.; Li, P.; Simpson, J. C.; Butler, G.; Lee, G. U. Characterization of carboxylate nanoparticle adhesion with the fungal pathogen Candida albicans. *Nanoscale* **2017**, *9*, 15911−15922.

(59) Beaussart, A.; Beloin, C.; Ghigo, J.-M.; Chapot-Chartier, M.-P.; Kulakauskas, S.; Duval, J. F. L. Probing the influence of cell surface polysaccharides on nanodendrimer binding to Gram-negative and Gram-positive bacteria using single-nanoparticle force spectroscopy. *Nanoscale* **2018**, *10*, 12743−12753.